Stem Cell Reports
Article
OPEN ACCESS

PGC-1α and Reactive Oxygen Species Regulate Human Embryonic Stem Cell-Derived Cardiomyocyte Function

Matthew J. Birket,[1] Simona Casini,[1] Georgios Kosmidis,[1] David A. Elliott,[5] Akos A. Gerencser,[2] Antonius Baartscheer,[3] Cees Schumacher,[3] Pier G. Mastroberardino,[4] Andrew G. Elefanty,[5,6] Ed G. Stanley,[5,6] and Christine L. Mummery[1,*]

[1]Leiden University Medical Center, 2300RC Leiden, The Netherlands
[2]Buck Institute for Research on Aging, Novato, CA 94945, USA
[3]Amsterdam Medical Center, 1105AZ Amsterdam, The Netherlands
[4]Erasmus Medical Center, 3015GE Rotterdam, The Netherlands
[5]Murdoch Childrens Research Institute, The Royal Children's Hospital, Flemington Road, Parkville, Victoria 3052, Australia
[6]Monash Immunology and Stem Cell Laboratories, Monash University, Wellington Road, Clayton, Victoria 3800, Australia
*Correspondence: c.l.mummery@lumc.nl
http://dx.doi.org/10.1016/j.stemcr.2013.11.008

SUMMARY

Diminished mitochondrial function is causally related to some heart diseases. Here, we developed a human disease model based on cardiomyocytes from human embryonic stem cells (hESCs), in which an important pathway of mitochondrial gene expression was inactivated. Repression of *PGC-1α*, which is normally induced during development of cardiomyocytes, decreased mitochondrial content and activity and decreased the capacity for coping with energetic stress. Yet, concurrently, reactive oxygen species (ROS) levels were lowered, and the amplitude of the action potential and the maximum amplitude of the calcium transient were in fact increased. Importantly, in control cardiomyocytes, lowering ROS levels emulated this beneficial effect of *PGC-1α* knockdown and similarly increased the calcium transient amplitude. Our results suggest that controlling ROS levels may be of key physiological importance for recapitulating mature cardiomyocyte phenotypes, and the combination of bioassays used in this study may have broad application in the analysis of cardiac physiology pertaining to disease.

INTRODUCTION

Pluripotent stem cells (PSCs) have the remarkable capacity to generate all cell types of the body (Thomson et al., 1998). Potential biomedical applications for the derivatives of PSCs are vast and diverse, including disease modeling, drug testing, tissue engineering, and cell therapies. However, to fully realize the potential of any of these applications, it is essential to understand more about their functional properties and to identify the factors that control their stability and maturation, since all differentiated derivatives of PSCs in vitro are immature, with fetal rather than adult characteristics (Murry and Keller, 2008).

Here, we were interested in examining the properties of cardiomyocytes derived in vitro from human embryonic stem cells (hESCs). Electrically and contraction-competent cardiomyocytes can now be generated efficiently under defined conditions from hESCs and human induced pluripotent stem cells (hiPSCs) (Mummery et al., 2012). These cardiomyocytes have the potential to be used for all of the applications relevant to heart physiology and disease mentioned above. Now that the efficiency of differentiation is not rate limiting, a deeper study of the cardiomyocyte function is feasible and warranted. Of particular relevance to the heart's function as a pump is the ability of the cardiomyocytes to supply themselves with the necessary energy for their work. During development in vivo, cardiomyocytes acquire a high density of mitochondria, which ultimately occupy 20%–30% of the cell volume in the adult (Schaper et al., 1980). This gives these cells a huge capacity for ATP synthesis, which is necessary to fund the high energy demands of ion pumping and contractility during strenuous activity. The importance of mitochondria for heart function is highlighted by the fact that functionally important mutations that affect mitochondria frequently cause cardiomyopathy (Bates et al., 2012; Hirano et al., 2001), and diminished mitochondrial function is an almost universal feature of cardiac disease (Ventura-Clapier et al., 2011).

Heart disease remains a major cause of morbidity and mortality in the Western world and there is an urgent need for better models and treatment strategies. Surprisingly, though, investigation of mitochondrial involvement in heart disease has largely been limited to mice, which have a markedly different cardiac physiology compared with humans (Davis et al., 2011) and have not proved to be a highly predictable model for mitochondrial disease. The advent of human PSC research has created opportunities to probe the functional relationship between mitochondria and heart failure, and to study the specific cardiac pathogenic mechanisms of mitochondrial diseases using iPSCs generated from patients. However, little is known

about how mitochondrial functions and bioenergetics change in the transition from a PSC to a cardiomyocyte, or how important these functions are. An analysis of these fundamental characteristics is thus warranted. Such an analysis would have practical implications for investigating the response to an energetic stress, such as a hypertrophic or chronotropic stimulus, and for studying disease phenotypes in which mitochondria are implicated, such as cardiomyopathy and cardiac hypertrophy.

Another important consideration is that if cardiomyocytes acquire a high density of highly polarized mitochondria, one would also expect reactive oxygen species (ROS) production to be high. It is not known what impact this would have on cardiomyocyte function, stability, or maturation in this in vitro context, and therefore whether ROS levels should be controlled. ROS have been shown to affect a variety of important ion channels and pumps, so the benefit of having a large energy reserve could be offset by a greater burden on the cell as a consequence of oxidative modifications and damage (Goldhaber et al., 1989; Liu et al., 2010; Zima and Blatter, 2006).

From a developmental perspective, if hPSC-derived cardiomyocytes do show developmentally related changes, this system could provide a robust model for learning about the regulation of these changes during formation of the human heart. For example, fundamental details such as whether the increase in cardiomyocyte mitochondria is driven primarily by energy demands or by a genetic program remain unknown. It is also not known which genes control mitochondrial biogenesis in human heart cells and whether these same genes are involved in heart disease. In the mouse, genes with known roles in mitochondrial biogenesis seem to have deterministic roles in heart failure (Fritah et al., 2010a), and some of these factors have also been additionally implicated in the perinatal maturation of the mouse heart (Lai et al., 2008).

In this study, we addressed fundamental aspects of hESC-derived cardiomyocyte bioenergetics and identified *PGC-1α* as a major regulator of mitochondria and wider functionality in these cells.

RESULTS

Differentiation of hESCs to Cardiomyocytes Involves a Large Increase in Mitochondrial Energy-Generating Capacity Despite Little Change in Cell Energetic Demand

We utilized the targeted *NKX2-5*$^{eGFP/w}$ hESC reporter line, in which enhanced GFP (hereafter referred to as GFP) is expressed in cardiac progenitors and cardiomyocytes (Dubois et al., 2011; Elliott et al., 2011), to analyze changes in the cellular bioenergetic status during differentiation toward fully committed (i.e., minimally proliferative) cardiomyocytes. We used this cell line in combination with the Seahorse Bioanalyzer to assess respiration and anaerobic glycolytic rates (proton production rates) in monolayer cultures (Figure 1). Fluorescence-activated cell sorting (FACS)-sorted embryoid body (EB)-derived cells (at day 12+7 postdifferentiation [D12+7]) contained 95.5% ± 3% cardiomyocytes in the GFPpos fraction and 11.5% ± 3% cardiomyocytes in the GFPneg fraction as assessed by troponin I immunofluorescence staining (Figure 1A). This is consistent with a subpopulation of NKX2-5neg cardiomyocytes in the heart (Christoffels et al., 2006). The GFPneg fraction is further composed of a heterogeneous population of mesodermal cell types (Figures S1A and S1B available online). In this monolayer format, the GFPpos cell population (hereafter referred to as cardiomyocytes) spontaneously contracted at a mean frequency of 0.50 ± 0.04 Hz.

hESCs actively respire, generating more than half of their ATP by oxidative phosphorylation (Birket et al., 2011). The hESC line used here also showed this bias, with an estimated 68% ± 4% of ATP generated by oxidative phosphorylation (Figures 1B–1D). Cardiomyocyte cultures (D12+7 GFPpos) showed a significant increase in coupled respiration, whereas the anaerobic glycolytic rate was significantly decreased, resulting in little difference in total ATP output. By contrast, the GFPneg population showed no change in coupled respiration, but the significantly decreased anaerobic glycolytic rate caused a reduction in total basal ATP output. However, mitochondrial inhibition by oligomycin increased anaerobic glycolysis in cardiomyocytes to a level as high as that observed in hESCs (Figure 1B). This shift in energy supply after oligomycin addition was permissive for contractility, demonstrating that anaerobic glycolysis is robust enough to support beating. In fact, contracting cardiomyocytes were produced even when mitochondrial ATP production was inhibited from day 3 of EB differentiation. Thus, this ATP source is not essential for cardiomyocyte differentiation either (Figure S1C).

To determine the component contributors to energy demand, we inhibited contraction and/or the action potential (AP) and calcium transient. Contraction was inhibited using the Myosin II ATPase inhibitor blebbistatin (Straight et al., 2003), which does not affect electrical excitability, and a combination of blebbistatin and the L-type calcium channel inhibitor nifedipine was used to additionally block the AP and the calcium transient. The difference between the effect of the blebbistatin alone and the combination of the two inhibitors should give the energy demand of only the AP and the calcium transient. These calculations showed that sarcomeric contraction alone accounted for

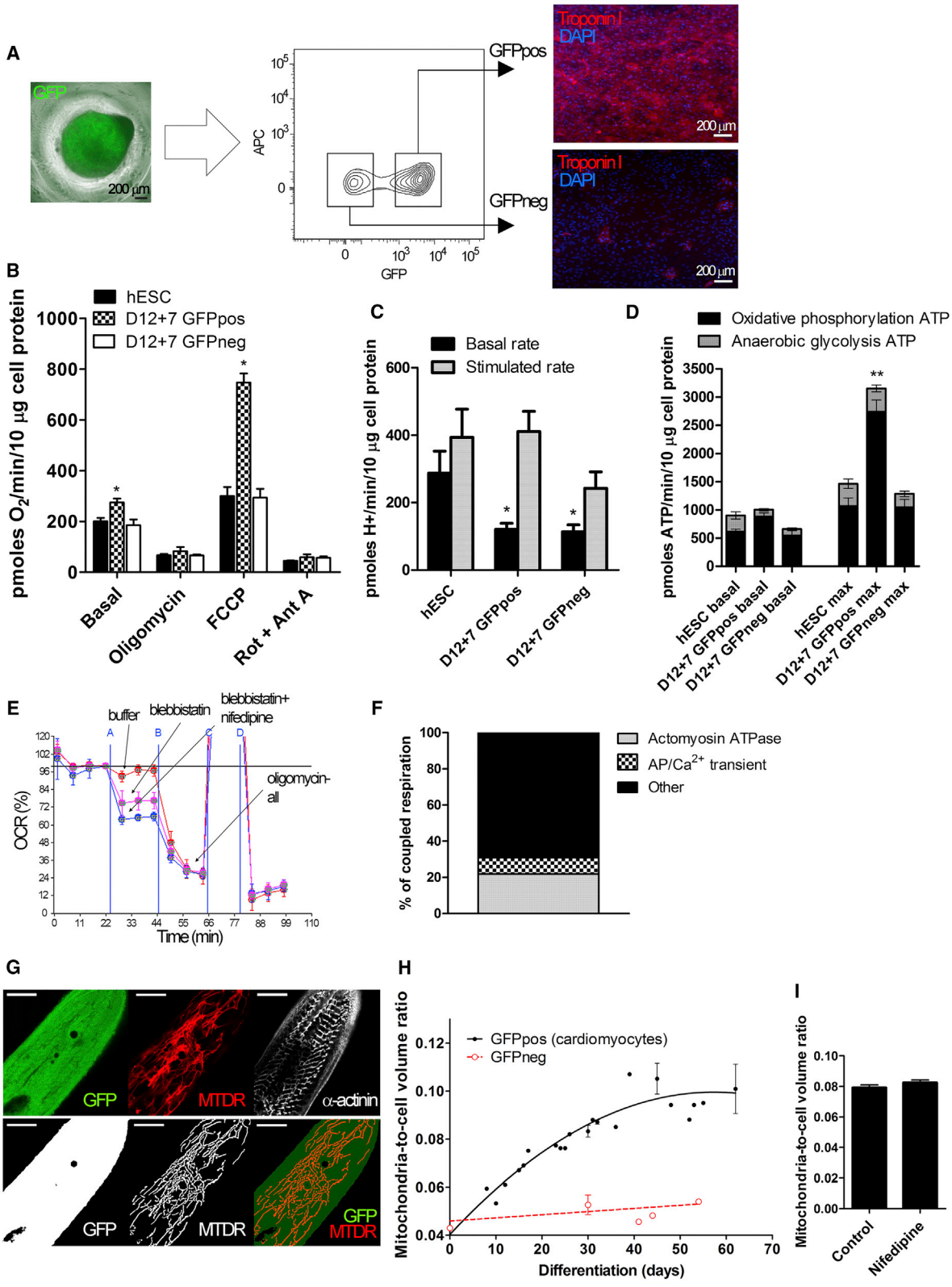

(legend on next page)

21.9% ± 1.9% of coupled respiration, and the AP and the calcium transient combined accounted for 9% ± 2.9% (Figures 1E and 1F).

An obvious bioenergetic difference between these three cell populations was the vastly increased maximal respiratory capacity, and thus the theoretical ATP production capacity, of the cardiomyocytes (Figure 1B and 1C). This suggests the possibility of increased mitochondrial respiratory chain content in these cells. Additionally, or alternatively, this could be due to changes in tricarboxylic acid (TCA) cycle enzymes, their state of activation, or differences in matrix [Ca^{2+}] between beating and nonbeating cells. To assess mitochondrial content changes, possibly relating to cell maturation, we calculated the mitochondria-to-cell volume ratio. From a typical dissociation at D12, there was clear evidence of a gradual time-dependent increase in mitochondria in cardiomyocytes (Figures 1G and 1H). By contrast, the GFPneg fraction showed very little evidence of increased mitochondrial biogenesis. As there was little overall increase in energy demand between the hESC state and the cardiomyocyte culture at D12+7, we reasoned that this process is unlikely to be driven in response to the basic energy demands of the cardiomyocyte. Supporting this prediction, the addition of nifedipine to reduce energy demand did not prevent the increase in mitochondria (Figure 1I).

This suggests that cardiomyocyte mitochondrial biogenesis might be regulated by a set developmental genetic program rather than occurring simply as a stochastic process in response to current energy requirements.

The Progressive Increase in Mitochondrial Volume in Developing Cardiomyocytes Is Driven by a Developmental Genetic Program Orchestrated by *PGC-1α*

Mitochondrial biogenesis is coordinated by the regulation of transcriptional coregulators that act on DNA-binding transcription factors to modulate the expression of nuclear-encoded mitochondrial genes (Fritah et al., 2010b; Scarpulla et al., 2012). We examined the expression profile of three coregulators: two activators (*PGC-1α* and *PGC-1β*) and one corepressor (*RIP140*). An obvious and universal feature was the large upregulation of *PGC-1α* specific to the GFPpos fractions with either "spin EB" differentiation or coculture differentiation using END2 cells (Figure 2A). Of the three genes, this was the only strong candidate, because *PGC-1β* was not upregulated in END2 coculture-derived cardiomyocytes and *RIP140* expression was elevated universally during differentiation. The spin EB cardiomyocyte gene-expression changes were mirrored during human heart development (Figure S2A). Furthermore, GFP expression was detectable by D7 (Figure 2B), corresponding exactly with the onset of *PGC-1α* expression (Figure 2C). In addition, *PGC-1α* expression was largely independent of energy demand related to cell contraction, as the induction was only marginally affected by the presence of nifedipine, consistent with the mitochondrial biogenesis phenotype (Figure 2D). Recently, four different isoforms of *PGC-1α* have been described, and although the primers used here were able to detect both *PGC-1α1* and *PGC-1α4*, isoform-specific PCR showed that *PGC-1α4* was

Figure 1. Vastly Increased Respiratory Capacity and Mitochondrial Volume in hESC-Derived Cardiomyocytes, with Little Change in Total Energy Demand

(A) Sorting of EB-derived cells in an NKX2-5 reporter line into GFPpos and GFPneg fractions. Troponin I staining of representative sorted populations.

(B) Oxygen consumption rates (OCRs) in monolayers of hESCs, D12+7 GFPpos, and D12+7 GFPneg sorted cells, normalized to cell protein levels. Basal, endogenous rate; oligomycin, ATP-synthase inhibited rate; FCCP, maximum stimulated rate; Rot + Ant A, rotenone- and antimycin A-inhibited rate.

(C) Anaerobic glycolytic rates at basal or oligomycin-inhibited state.

(D) ATP production rates from oxidative phosphorylation or anaerobic glycolysis under basal conditions or at the maximum stimulated rate.

(E) OCR plot during addition of blebbistatin or nifedipine+blebbistatin followed by oligomycin to calculate ATP demand for excitation/contraction. Drug additions are marked A–D as described in Experimental Procedures.

(F) ATP demand "budget" of contracting cardiomyocytes, showing the proportion of coupled oxygen consumption used by different processes (n = 3 independent experiments).

(G) Imaging for mitochondria-to-cell volume calculations in cardiomyocytes. Live-cell images of GFP or MitoTracker Deep Red (MTDR) are shown in the upper panel, and processed images are shown in the lower panel. α-Actinin staining in the same cell after fixation confirms cardiomyocyte identity (top-right image). The scale bar represents 10 μm.

(H) Mitochondria-to-cell volume ratios in GFPpos and GFPneg cells during differentiation from hESCs.

(I) Mitochondria-to-cell volume ratios in GFPpos cells at D30 cultured in the presence or absence of nifedipine (n = 3 independent experiments). Data are represented as mean ± SEM. Statistical significance was calculated using a one-way ANOVA with Dunnett's correction and hESC values as control in (A)–(C), and data are presented as mean values from three to five independent experiments for each cell type ± SEM. *$p < 0.05$.

See also Figure S1.

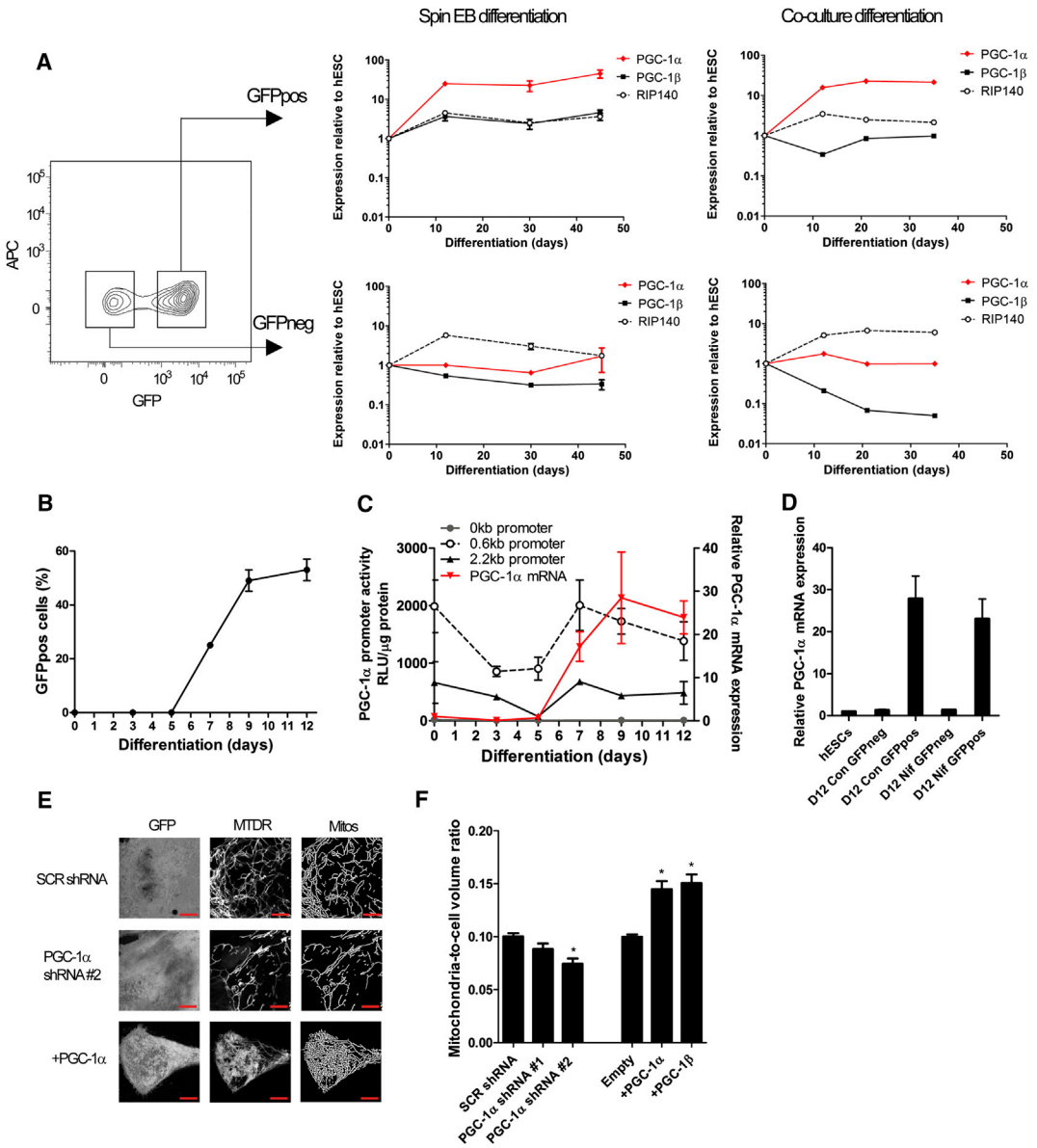

Figure 2. Mitochondrial Biogenesis Is Driven by PGC-1α during Cardiac Differentiation Independently of Energy Demand for Excitation/Contraction

(A) Cell sorting following cardiac differentiation via either spin EB or coculture protocols to separate GFPpos and GFPneg populations for RNA isolation. Normalized gene expression is shown relative to hESCs for *PGC-1α*, *PGC-1β*, and *RIP140* from these sorted GFPpos and GFPneg populations.

(B) GFPpos cell induction during early EB cardiac differentiation.

(C) Induction of *PGC-1α* mRNA in whole EBs during cardiac differentiation, and the parallel activity of three *PGC-1α*-luciferase reporter constructs of 0 kb, 0.6 kb, and 2.2 kb promoter lengths.

(D) *PGC-1α* mRNA in sorted populations at D12 from EBs differentiated in the presence or absence of nifedipine (Nif).

(E) Images of cardiomyocytes showing GFP, MitoTracker Deep Red (MTDR), and processed MTDR in cells (mitos) transduced 7 days before with Scr shRNA as control, a *PGC-1α*-specific shRNA (#2), and a lentivirus for overexpression of *PGC-1α*. Scale bar represents 10 μm. In (A)–(D), data are represented as mean ± range (n = 2 independent experiments).

(F) Quantifications of the mitochondria-to-cell volume ratio measured after 7 days. Data are represented as mean ± SEM (n = 4 independent experiments). Statistical significance was calculated using a one-way ANOVA with Dunnett's correction using Scr shRNA or empty vector as controls. *p < 0.01.

See also Figure S2.

not detectable in our cells (Figure S2B) and the upregulation was of *PGC-1α1*, which is the isoform that is most important for mitochondrial biogenesis (Ruas et al., 2012). Although many transcription-factor-binding elements have been studied within the *PGC-1α1* proximal promoter and shown to coordinate its regulation, neither a 2.2 kb nor a 0.6 kb promoter was sufficient to drive elevated luciferase expression at D7 (Figure 2C), suggesting more complex regulation. Stronger activity from the 0.6 kb promoter is consistent with the possible presence of repressive elements upstream of position −823 (Irrcher et al., 2009).

To test the involvement of *PGC-1α* in the cardiomyocyte-specific mitochondrial changes, we stably expressed short hairpin RNAs (shRNAs) targeting *PGC-1α* or a scrambled (Scr) control from D12, and assessed cardiomyocyte mitochondrial volume after 7 days of gene knockdown. The efficacy of the shRNAs was confirmed (Figure S2C). Clone shRNA #2 significantly inhibited mitochondrial biogenesis in cardiomyocytes and shRNA #1 also marginally diminished its rate (Figures 2E and 2F). Constitutive overexpression of *PGC-1α* or *PGC-1β* resulted in a dramatic increase in mitochondrial volume. Together, these data show that *PGC-1α* plays an important role in the normal induction of mitochondrial biogenesis in these cardiomyocytes. Further, *PGC-1β* may be able to functionally substitute for *PGC1α* even though it does not act during normal cardiogenesis in this system.

PGC-1α Plays a Key Role in Regulating hESC-Derived Cardiomyocyte Mitochondrial Respiration, Contractile Automaticity, and Superoxide Production

To assess how depletion of *PGC-1α* affects mitochondrial function, we performed a bioenergetic analysis 7 days after gene knockdown. Both *PGC-1α* shRNA sequences repressed mitochondrial respiration, with a very dramatic decrease in maximal respiration for shRNA #2, confirming that this gene alone plays a major role in increasing energy-generating capacity during cardiac differentiation (Figure 3A). Surprisingly, the basal ATP turnover in these cells was also diminished by *PGC-1α* knockdown despite considerable reserves in respiratory capacity, which means that these cardiomyocytes are doing less work (Figure 3B). Consistent with the diminished ATP turnover, the beating frequency was reduced by around 50% (Figure 3C). Therefore, the 25% reduction in ATP turnover following *PGC-1α* knockdown may be largely explained by the reduced frequency in excitation/contraction. Thus, PGC-1α seems to be an important regulator of cardiomyocyte contractile automaticity. The slower beating rate will result in decreased mitochondrial [Ca^{2+}], potentially decreasing TCA cycle activity. Lower ATP demand and lower mitochondrial [Ca^{2+}] could both be contributing to the decreased respiration rate.

Mitochondria are important producers of reactive oxygen species (ROS), which can be highly damaging and inhibitory to cardiomyocyte function. PGC-1α will increase the number of potential ROS-producing sites and may impact the rate of ROS production at these sites via changes in mitochondrial proton motive force. Figure 3D shows that in line with differential accumulation of the cationic probe tetramethylrhodamine methyl ester (TMRM) between GFPpos and GFPneg cells during normal EB differentiation, probably reflecting the change in mitochondria-to-cell volume ratio (Figure 1H), the levels of superoxide measured by dihydroethidium (DHE) were also different, increasing in cardiomyocytes and decreasing slightly in the GFPneg fraction. Knockdown of *PGC-1α* was sufficient to repress superoxide production in cardiomyocytes, effectively eliminating the difference between the populations (Figure 3E).

Additionally, oxidative stress proved to be an important second regulator of mitochondrial biogenesis in hESC-derived cardiomyocytes. Decreasing ROS levels by culturing the cells under 3% O_2 slowed the rate of mitochondrial biogenesis, whereas increasing ROS with low concentrations of rotenone, antimycin A, or H_2O_2 stimulated it (Figures S3A and S3B). *PGC-1α* mRNA is already elevated at D7 (Figure 2C), whereas superoxide increases only after this time (Figure 3D), excluding the possibility that ROS are primarily responsible for at least the initial elevation in *PGC-1α* mRNA and consequential PGC-1α-dependent mitochondrial biogenesis, consistent with an equal upregulation of *PGC-1α* with differentiation at 3% O_2 (Figure S3C). However, the ability of PGC-1α to stimulate ROS production may act to potentiate mitochondrial biogenesis, thereby reinforcing its action.

Given the striking effect of *PGC-1α* knockdown on the bioenergetics and ROS levels of cardiomyocytes, an investigation of the AP and the calcium transient was warranted.

PGC-1α Knockdown Alters AP Characteristics and Increases the Amplitude of the Calcium Transient via a Reduction in Oxidative Stress

Figures 4A and 4B show typical APs of clusters and single cardiomyocytes with control and *PGC-1α* knockdown; average AP parameters are summarized in Figure 4C. Clusters of cardiomyocytes as well as single cells were measured to avoid limiting the analysis to a subset of cells. Clusters show more robust activity during patch-clamp analysis, which could make them less prone to potential sampling bias.

In spontaneously beating cell clusters, the reduction in frequency remained evident upon *PGC-1α* knockdown (1.11 ± 0.42 versus 1.47 ± 0.30 Hz; Figures 4A and 4C).

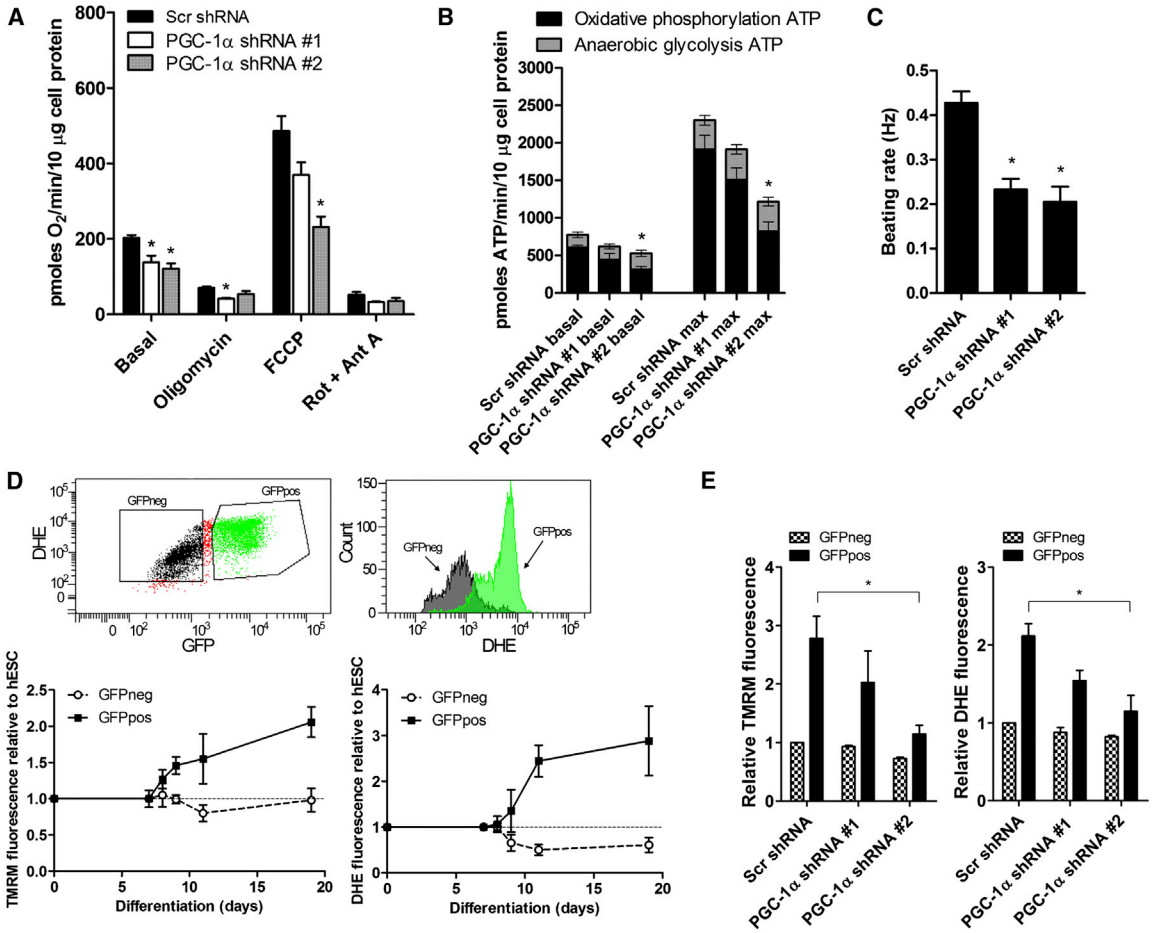

Figure 3. PGC-1α Is Responsible for Increased Respiratory Capacity in Cardiomyocytes, but Also Regulates Basal ATP Turnover and ROS Production

(A) OCRs in monolayers of cardiomyocytes transduced with shRNA-expressing lentivirus on D12 and measured 7 days later, with values normalized to cell protein levels. Basal, endogenous rate; oligomycin, ATP-synthase-inhibited rate; FCCP, maximum stimulated rate; Rot + Ant A, rotenone- and antimycin A-inhibited rate.

(B) ATP production rates from oxidative phosphorylation or anaerobic glycolysis under basal conditions or at the maximum stimulated rate.

(C) Average beating rates of cardiomyocyte monolayers used for bioenergetic analysis.

(D) TMRM and DHE FACS quantifications in GFPpos and GFPneg cells during EB differentiation. The dot plot and corresponding histogram show DHE-labeled cells gated based on GFP expression.

(E) TMRM and DHE FACS quantifications in cells transduced with shRNA-expressing lentivirus. Values are relative to the GFPneg cells in the control Scr shRNA. All data are represented as mean ± SEM; n = 4 independent experiments in (A)–(C) and (E), and 3 independent experiments in (D). Statistical significance was calculated using a one-way ANOVA with Dunnett's correction. *$p < 0.05$.

See also Figure S3.

The faster rates compared with those measured in the Seahorse plates (Figure 3C) may reflect the different experimental conditions (see Experimental Procedures).

The maximal diastolic potential (MDP) and AP upstroke velocity did not differ significantly. However, AP amplitude was significantly increased on *PGC-1α* knockdown in both single cells (109 ± 2 versus 101 ± 2 mV; p = 0.013) and clusters (116 ± 2 versus 107 ± 2 mV; p = 0.009). Furthermore, AP duration was prolonged in both groups, although only statistically significant in clusters (APD_{50} = 153 ± 15 versus 102 ± 17 ms, p = 0.034; APD_{90} = 182 ± 16 versus 120 ± 17 ms, p = 0.015; Figure 4C).

To assess whether the changes in the AP following *PGC-1α* knockdown could be mimicked by direct mitochondrial inhibition, the mitochondrial ATP synthase inhibitor oligomycin was added to the extracellular solution during measurement of clusters of control cardiomyocytes. Neither frequency nor any other parameter of the AP was

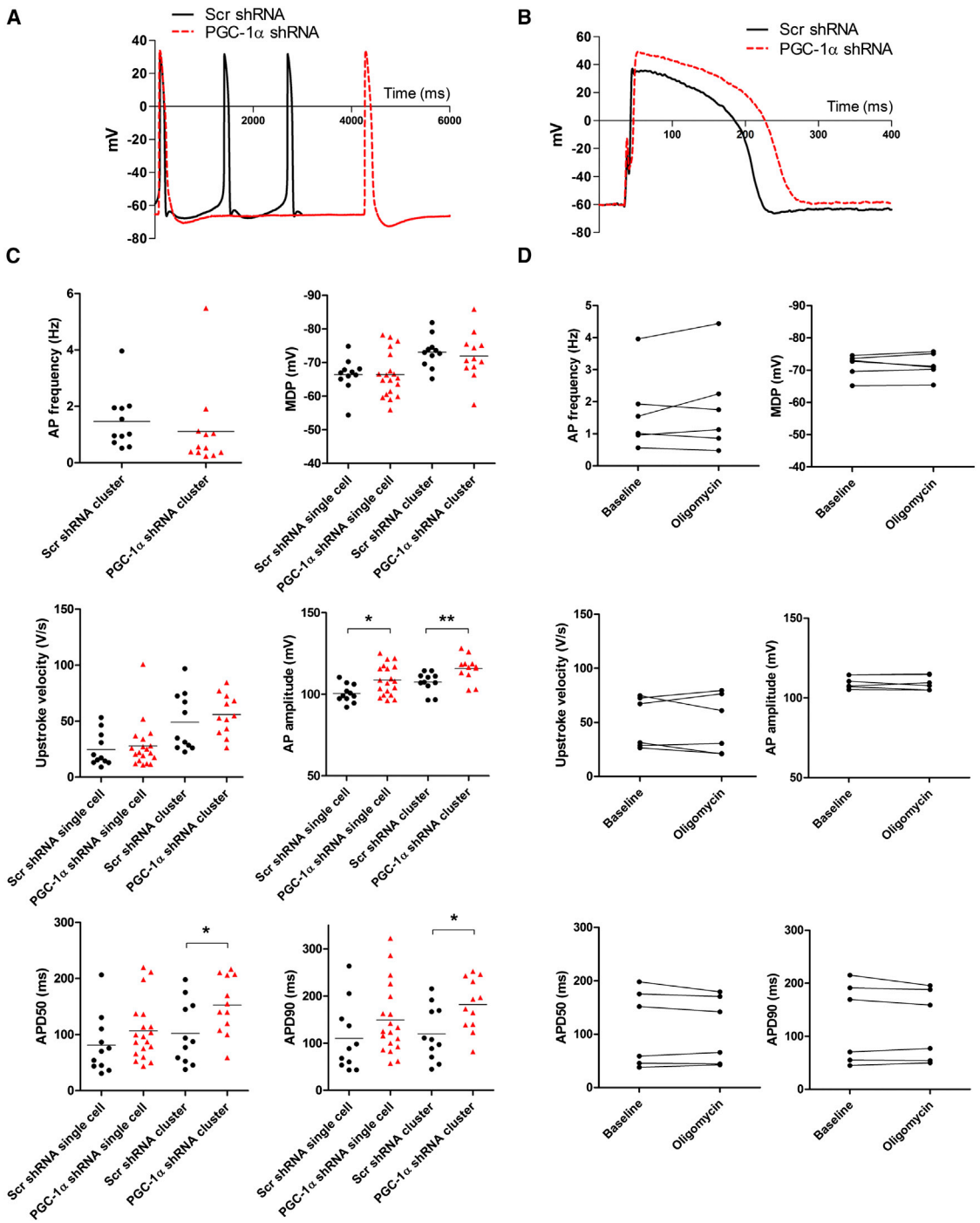

Figure 4. AP Characteristics with *PGC-1α* Knockdown or Mitochondrial Inhibition

(A) Typical spontaneous APs in clusters of cells previously transduced with a control Scr shRNA or the *PGC-1α*-specific shRNA.

(B) Typical APs elicited at 1 Hz in single cardiomyocytes.

(C) Average AP characteristics.

(D) AP parameters in spontaneously beating clusters of control cardiomyocytes at baseline or following perfusion with oligomycin. APD_{50} and APD_{90} = AP duration at 50% and 90% repolarization, respectively. Statistical significance was calculated using an unpaired or paired t test in (C) and (D), respectively. *$p < 0.05$.

See also Figure S4.

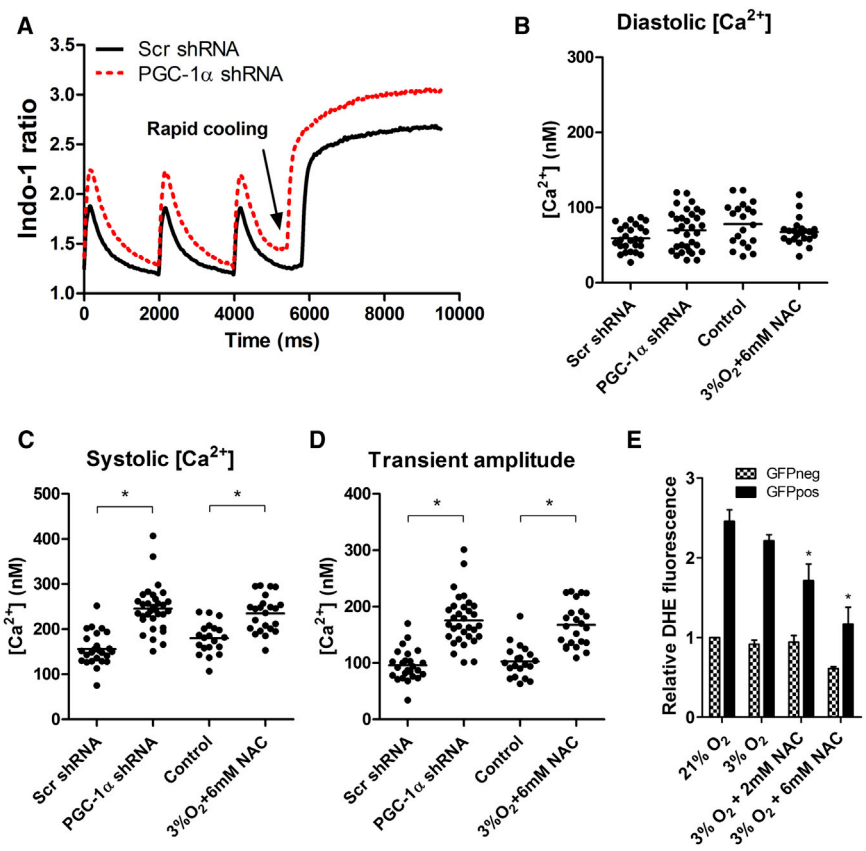

Figure 5. Calcium Transient Characteristics with *PGC-1α* Knockdown and the Effect of Directly Lowering ROS Levels

(A) Indo-1 ratio values showing transients in paced cardiomyocyte clusters and the response to rapid cooling.

(B–D) Average diastolic (B), systolic (C), and transient (D) concentrations in cardiomyocyte clusters paced at 0.5 Hz. Statistical significance was calculated using an unpaired t test (data are from three independent experiments).

(E) Superoxide levels measured by DHE following 5 days under test conditions of control (21% O_2), low oxygen (3% O_2), or low oxygen plus NAC. Data are represented as mean ± SEM (n = 3 independent experiments). Statistical significance was calculated using a one-way ANOVA with Dunnett's correction using the 21% O_2 GFPpos values as the control. *p < 0.05. See also Figure S5.

significantly affected by application of oligomycin for 4 min (Figure 4D). Contraction frequency was also unchanged when measured by imaging after exposure to oligomycin for 15 min in normal culture conditions (Figure S4). This suggests that ATP generated by anaerobic glycolysis alone may be sufficient to fund the AP requirements of these cells, at least in the short term, and that the effect of *PGC-1α* knockdown on the AP may not necessarily be related to the energetic defect in these cells.

Figure 5A shows typical $[Ca^{2+}]_i$ measurements in a control and a *PGC-1α* knockdown cluster; average $[Ca^{2+}]_i$ values are summarized in Figures 5B–5D. The diastolic $[Ca^{2+}]_i$ was similar between control and *PGC-1α* knockdown clusters (Figure 5B). However, systolic $[Ca^{2+}]_I$ was increased (Figure 5C) and consequently the Ca^{2+} transient (Figure 5D) was larger in *PGC-1α* knockdown clusters. The positive response to rapid cooling to release sarcoplasmic reticulum (SR) calcium suggests that the SR is a major store of Ca^{2+} in both conditions (Figure 5A).

The increase in systolic calcium is unlikely to be due to a lower level of calcium buffering by mitochondria, as mitochondria are reported to remove only 1% of systolic calcium even in adult myocytes during a transient (Bassani et al., 1994; Bers, 2008). We tested whether the effect on $[Ca^{2+}]_i$ could be recreated by lowering ROS levels. Incubation at 3% O_2 in the presence of 6 mM N-acetyl cysteine (NAC) suppressed superoxide levels in cardiomyocytes to a value equivalent to that observed for *PGC-1α* knockdown cardiomyocytes (53% versus 56% decrease, respectively; Figure 5E). In cells precultured in this low-ROS condition, the Ca^{2+} transient was similarly increased (Figures 5B–5D). The same changes were evident when the clusters were paced at 1 Hz (Figure S5), although the decreased transient in all conditions at 1 Hz already reveals a negative force-frequency relationship above 0.5 Hz.

PGC-1α Is Important for the Maintenance of Cardiomyocyte Sarcomeric Organization during Fetal Calf Serum-Induced Hypertrophy and Response to Beta-Adrenergic Stimulation

Under baseline conditions, where these cardiomyocytes are using only about one-third of their theoretical ATP production capacity (Figure 1C), mitochondrial function may be partially redundant. However, under more energy-demanding conditions, one would expect that an energetic compromise might be exposed. To investigate this possibility, we established a model of cardiomyocyte hypertrophy using fetal calf serum (FCS) as the inducing agent. We found that 5% FCS caused a hypertrophic phenotype resulting in a volume difference of 3.8-fold

when measured after 18 days (Figures 6A and 6B), from a median of 2,324 μm^3 in serum-free media (BSA, polyvinyl alcohol, essential lipids [BPEL]) to 8,886 μm^3 in 5% FCS (n = 85 and 78 cells, respectively; $p < 0.001$). The question we wanted to address was whether *PGC-1α*-depleted cells would still be able to maintain their structural organization during this volume increase by correctly synthesizing, trafficking, and recycling their specialized sarcomeric proteins. Following NKX2-5pos cell identification in live cells, α-actinin staining was used to categorize single cardiomyocytes into three structural classes (Figure 6C). In class I, α-actinin antiparallel bands are present across more than half of the cell's area; in class II, many bands are also present but across less than half of the cell's area; and in class III, labeling is apparent but a banding pattern is almost completely absent. In cardiomyocytes transduced with the control Scr shRNA, 17.6% were of the class III type after chronic FCS exposure, whereas in *PGC-1α*-depleted cardiomyocytes, a significantly higher proportion (53.5%; chi-square test, $p < 0.001$) displayed class III characteristics (Figure 6D). Chronic incubation with the mitochondrial uncoupler 2,4-dinitrophenol (DNP) caused a similar disturbance to structural integrity, suggesting that energetic compromise may be the cause of this phenomenon (Figure 6E; chi-square test, $p < 0.001$).

In a second assay, we evaluated the chronotropic response to beta-adrenergic stimulation. We found that 100 nM of isoproterenol raised the spontaneous beating frequency of Scr shRNA control cardiomyocyte clusters in 30 of 33 areas by a mean increase in rate of 79% (Figure 6F). In *PGC-1α* knockdown clusters, isoproterenol caused beating to cease completely in 29 of 48 areas, while 17 areas increased their rate by a mean of 74% (Figure 6G). Consistent with the imaging data, isoproterenol increased the ATP production rate of the Scr shRNA control cells by 43.5% with both increased oxidative phosphorylation and anaerobic glycolysis, whereas in *PGC-1α* shRNA cells, ATP production rate was decreased overall by 19% (Figure 6H). The increased glycolytic rate in these *PGC-1α* shRNA cells by isoproterenol may reflect a much faster rate in the minority of cells that were able to increase their beating frequency under this condition.

DISCUSSION

In this study, we have described the bioenergetics of hESC-derived cardiomyocytes and the functional impact of its manipulation. Our principal finding is that upon induction of cardiac differentiation in hESCs, a *PGC-1α*-dependent developmental program was engaged that strongly stimulated mitochondrial biogenesis, consistent with cardiomyocyte maturation. Inactivating this pathway blocked mitochondrial biogenesis, but also lowered levels of ROS. This led to an increased AP and calcium transient amplitude, and at the same time made these cells vulnerable to metabolic stress.

Cardiomyocytes are rather unique in that during embryonic and fetal development, they undergo dramatic maturation-related changes, progressing from small rounded cells with immature sarcomeric organization and limited energy-generating capacity to large rectangular cells with dense striated myofibrils organized in parallel to densely packed elongated mitochondria (Martin-Puig et al., 2008; Piquereau et al., 2010). Cardiomyocyte mitochondria are essential for supplying the ATP required for excitation/contraction during intense heartbeating, and if respiratory function is compromised as a result of mutation or damage, or is dysregulated in other ways, there may be pathological consequences (Arany et al., 2005; Bates et al., 2012; Graham et al., 1997).

Much of what we know about the genetics of mitochondrial regulation in the heart still comes from the mouse. Widely regarded as mitochondrial gene "master regulators," *PGC-1α* and *PGC-1β* are known to be highly expressed in the heart, and overexpression of *PGC-1α* has been shown to induce mitochondrial proliferation in both the mouse heart and cultured rat cardiomyocytes (Lehman et al., 2000; Russell et al., 2004). Single *PGC-1α* or *PGC-1β* gene deletions have only a mild effect on the increase in mitochondrial mass that normally occurs during heart development, and the cardiac phenotypes are subtle, often becoming apparent only under metabolic challenge (Arany et al., 2005; Gurung et al., 2011; Lelliott et al., 2006; Leone et al., 2005). By contrast, the hearts of *PGC-1α/β* double-knockout mice are severely affected; the mice die soon postnatally and have markedly diminished mitochondrial mass and density even though up to mid-gestation, the mitochondria are apparently normal (Lai et al., 2008). This suggests that other, *PGC-1*-independent mitochondrial biogenesis-promoting genes may be involved in early mouse heart development.

Our system models human cardiac mitochondrial biogenesis using nontransformed cells, allowing this process to be studied in parallel with function. We found that *PGC-1α* alone was strongly upregulated at the very initiation of cardiac differentiation specifically in NKX2-5pos cells, regardless of the differentiation method used. The cardiomyocytes showed a regular and progressive increase in mitochondrial mass over many weeks of culture that depended on *PGC-1α*. Mitochondrial expansion still occurred in the complete absence of excitation/contraction, demonstrating that cardiomyocyte identity is linked to the mitochondrial biogenesis phenotype irrespective of increased energy demand. Significantly raising the energy demand may stimulate it further, as we observed

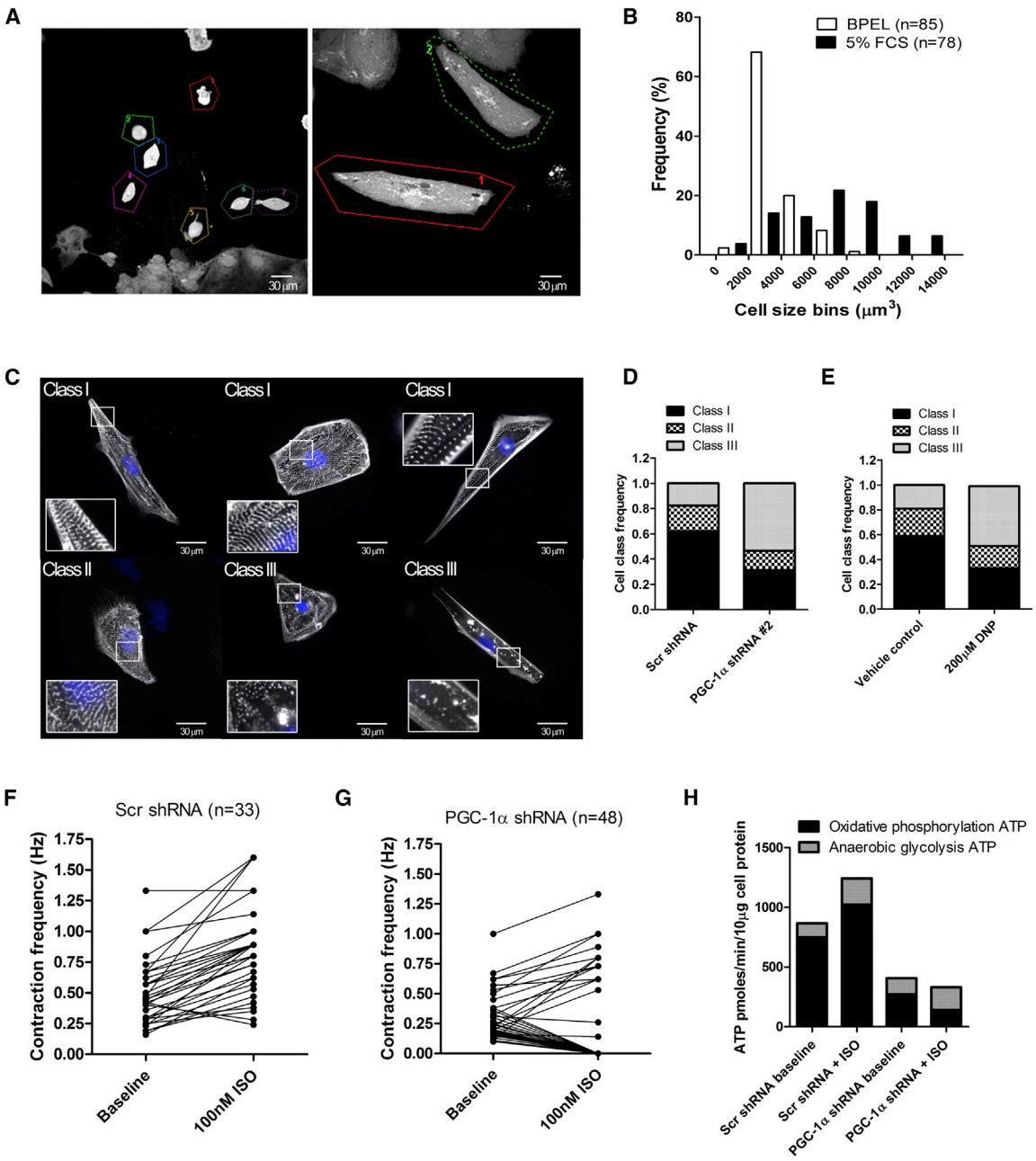

Figure 6. PGC-1α Is Important for Maintaining Cardiomyocyte Structural Identity during FCS-Induced Hypertrophy and for the Chronotropic Response to Beta-Adrenergic Stimulation

(A) Calcein-AM-labeled cells used for cell volume calculations, previously maintained for 18 days in serum-free BPEL media (i) or 5% FCS-containing media (ii). GFPpos cardiomyocytes were identified before loading and are shown as regions of interest.

(B) Histogram quantification of cell volumes for the two culture conditions. BPEL median = 2324 μm^3 (n = 85), 5% FCS median = 78 μm^3 (n = 78); $p < 0.001$.

(C) α-Actinin-labeled NKX2-5pos cells (cultured in 5% FCS) classified by sarcomeric structure into three groups.

(D) Frequency of each cardiomyocyte structural class in Scr shRNA and *PGC-1α*-specific shRNA conditions (n = 160 cells counted from 3 independent experiments).

(E) Frequency of each cardiomyocyte structural class in vehicle control cells compared with 200 μM DNP-treated cells (n = 80 cells counted from 2 independent experiments).

(F) Contraction frequency of individual Scr shRNA-transduced clusters at baseline and after exposure to 100 nM isoproterenol.

(legend continued on next page)

with DNP (Figure S3), but was not essential for the basal rate of mitochondrial biogenesis.

Since mitochondria are a principal source of ROS production, we also investigated whether *PGC-1α*-dependent mitochondrial changes result in altered ROS levels in cardiomyocytes. Although PGC-1α can induce the expression of antioxidant enzymes (St-Pierre et al., 2006), in this context the impact of having a greater number of mitochondrial ROS-producing sites must outweigh the induction of detoxification pathways, because ROS levels were increased.

Remarkably, upon *PGC-1α* knockdown, the amplitude and duration of the AP and the maximum amplitude of the calcium transient were increased to values closer to those found in adult cardiomyocytes, despite a marked energetic defect. Energetic compromise in cardiomyocytes typically shortens the AP as a result of increased ATP-regulated potassium current, and decreases the calcium transient amplitude (Baartscheer et al., 2011; Koumi et al., 1997; Nichols et al., 1991). Yet, counter to this, there is evidence for an inhibitory effect of oxidative stress on the calcium current and AP duration (Goldhaber et al., 1989; Guerra et al., 1996). Given our evidence for the oligomycin insensitivity (at least upon short-term exposure) of the AP in these early cardiomyocytes, the benefit of lowered oxidative stress may be dominant in determining the overall outcome. Remarkably, repression of the mitochondrial biogenesis program in these cells resulted in an improvement in the calcium transient. Fortunately, however, the ROS levels could be lowered directly in control cardiomyocytes with a combination of culture at physiological oxygen tension and antioxidant supplementation, resulting in an improvement in the calcium transient to the same degree as *PGC-1α* knockdown. Based on these data, it may be worthwhile to make this a standard aspect of PSC-derived cardiomyocyte culture, at least at later stages of differentiation. Although an increase in mitochondrial mass is a feature of maturity, if the ROS produced by the mitochondria are not controlled, the overall function and contractility of the cardiomyocytes may be restricted. Further work will be required to determine precisely how ROS should be manipulated temporally to control the balance between maturation-related mitochondrial biogenesis and wider cell function.

Increasing the energetic demands of the cardiomyocytes through stimulation with FCS, and exerting physiologically relevant chronotropic stimulation through beta-adrenergic receptor activation both exposed shortcomings in *PGC-1α* knockdown cardiomyocytes. FCS induced a consistent hypertrophic growth, and in cells that had repressed *PGC-1α* or were uncoupled by DNP, this resulted in sarcomeric disorganization, presumably as a multifactorial response to inadequate energy supply. The mechanisms underlying the *PGC-1α*-dependent loss of automaticity upon isoproterenol stimulation, as well as the lower AP frequency under basal conditions, are unknown. They may relate to the longer AP we observed in these cells, the chronic energy disturbance, or an unknown connection between *PGC-1α* and automaticity. In line with this, both *PGC-1α* and *PGC-1β* knockout mouse hearts show blunted responses to beta-adrenergic stimulation with dobutamine, and it has been suggested they may be required for maximal automaticity of pacemaker cells, although a mechanism is lacking (Arany et al., 2005; Lelliott et al., 2006; Leone et al., 2005).

We set out to develop a human model of acquired heart disease by diminishing mitochondrial function. The rationale for this stemmed from the large body of literature reporting downregulation of mitochondrial pathways during heart failure, but with little explanation for how and why this occurs, or what consequences it has for individual heart cells (Ventura-Clapier et al., 2011). We confirmed that hESC-derived cardiomyocytes are a valuable tool for exploring the functional relationships between mitochondria and heart disease, revealing perhaps unexpected outcomes. Such studies go hand in hand with the goal of producing more adult-like cells for these and other applications. To maximize the potential function of these cells, it is important to control ROS, since the mitochondrial biogenesis program is activated in PSC-derived cardiomyocytes.

EXPERIMENTAL PROCEDURES

Cell Culture and Differentiation

Previously generated NKX2-5$^{eGFP/w}$ hESCs (Elliott et al., 2011) were maintained on mouse embryonic fibroblasts and passaged using TrypLE Select (Invitrogen). Differentiations were performed in serum-free media (BSA, polyvinyl alcohol, essential lipids [BPEL]) as previously described (Ng et al., 2008). The following growth factors were present for the first 3 days of differentiation: 35 ng/ml bone morphogenetic protein 4, 30 ng/ml activin A, 30 ng/ml vascular endothelial growth factor, and 40 ng/ml stem cell factor plus the GSK-3β inhibitor ChiR 99021 (1.5 μM). The Tankyrase inhibitor XAV 939 (1 μM) was present on D3–D6. Coculture

(G) Contraction frequency of individual *PGC-1α* shRNA-transduced clusters at baseline and after exposure to 100 nM isoproterenol.
(H) ATP production rates from oxidative phosphorylation or anaerobic glycolysis under basal conditions or after isoproterenol exposure (data represent the mean from four technical replicates). Statistical significance was calculated using an unpaired t test in (B) and a chi-square test in (D) and (E).

differentiations were performed as previously described (Mummery et al., 2007).

EBs typically were dissociated on D12 using TrypLE Select and plated onto plastic or glass coated with Matrigel (Invitrogen).

Lentiviral Transduction

PGC-1α and *PGC-1β* were overexpressed from a pLenti CMV/TO Puro DEST (Campeau et al., 2009; Addgene plasmid: 17452). The empty vector was used as the control. shRNAs against *PGC-1α* were obtained from Open Biosystems in the pLKO Puro vector (TRCN0000001167 [#1] and TRCN0000001166 [#2]). Scr shRNA was used as control (Addgene plasmid: 1864). The vectors used for luciferase measurements are described in the Supplemental Experimental Procedures.

Respiration and Acidification Rates Measured with the Seahorse XF-24 Analyzer

Respiration and acidification rates were measured on adherent cells using a Seahorse XF-24 analyzer (Seahorse Bioscience) as previously described (Birket et al., 2011). When combined with shRNA transductions, virus was added on cell plating at an appropriate titer to infect >90% of cells.

Basal acidification rates were taken as the mean rate from the second and third baseline readings, and "Max/stimulated" rates were taken after oligomycin addition. ATP production rates were calculated as previously described (Birket et al., 2011). Maximal ATP production rates ("Max") were calculated from the oxygen consumption rate difference between the oligomycin rate and the carbonyl cyanide p-(trifluoromethoxy)phenylhydrazone (FCCP) rate, and from the maximum extracellular acidification rate with oligomycin. At least three separate experiments were performed for each cell population.

For ATP demand calculations, normal untransduced cardiomyocytes were used with the experiment set up as above. After four baseline measurements, blebbistatin (5 μg/ml) or nifedipine (10 μM) plus blebbistatin, or DMSO was injected and the next measurement was used for the "process-inhibited" state. This was followed by oligomycin, FCCP, and rotenone and antimycin A injections. The fraction of oligomycin-sensitive respiration that was responsive to the drugs was calculated and the effect of the buffer-alone injection was subtracted.

Confocal Imaging of Mitochondria-to-Cell Volume Ratios

Cells were loaded with 40 nM MitoTracker Deep Red (Invitrogen) and imaged live in the presence of 10 μM nifedipine on a Leica SP5 confocal microscope. hESCs and GFPneg cells were also loaded with calcein-acetomethoxy (calcein-AM; 1 μM) to image the cell volume. Image acquisition and data analysis were performed as previously described (Birket et al., 2011).

Confocal Imaging for Calculation of Cell Volume

Cells were imaged live in the presence of 10 μM nifedipine on a Leica SP5 confocal microscope within a 37°C chamber using a Plan-Apochromat 40×/1.25 oil lens. Sequential imaging stacks were acquired through the entire thickness of calcein-AM-loaded cardiomyocytes and their volumes were calculated by calibration to 4 μm TetraSpek fluorescent microsphere standards (Invitrogen) imaged in the same way. Further details are described in the Supplemental Experimental Procedures.

ROS and TMRM Measurements

For ROS measurements, cell cultures were dissociated with TrypLE Select and labeled for 30 min at 37°C with 20 μM DHE (Molecular Probes). They were then washed twice with buffer and measured immediately by FACS. For TMRM measurements, 5 nM TMRM (Invitrogen) was added in BPEL media the day before measurement. Cells were dissociated as above, but with TMRM included in all solutions and also present during measurement.

Electrophysiological Characterization

APs were measured 7–15 days after cell dissociation via the amphotericin-perforated patch-clamp technique using an Axopatch 200B amplifier (Molecular Devices). Signals were filtered and digitized at 5 and 40 kHz, respectively. Data acquisition and analysis were accomplished using pClamp10.1 (Axon Instruments) and custom software. Potentials were corrected for the liquid junction potential.

APs were recorded at 37°C using Tyrode's solution containing (mM) NaCl 140, KCl 5.4, $CaCl_2$ 1.8, $MgCl_2$ 1.0, glucose 5.5, HEPES 5 pH 7.4 (NaOH). Pipettes (borosilicate glass; resistance ~2.5 MΩ) were filled with solution containing (mM) K-gluconate 125, KCl 20, NaCl 5, amphotericin-B 0.22, HEPES 10 pH 7.2 (KOH). APs were recorded from single cardiomyocytes as well as from small clusters of cardiomyocytes. The clusters were spontaneously active, whereas in single cardiomyocytes the APs were elicited by 3 ms 1.2× threshold current pulses through the patch pipette at 1 Hz. AP parameter values obtained from ten consecutive APs were averaged and data were collected from at least three independent differentiations per condition.

Calcium Imaging

Intracellular Ca^{2+} ($[Ca^{2+}]_i$) was measured at 37°C in Indo-1-loaded clusters of cardiomyocytes. In brief, cardiomyocytes were loaded with 5 μM of the fluorescent dye Indo-1-AM (Molecular Probes) for 50 min at 37°C in Tyrode's solution. The cardiomyocyte clusters were stimulated at 0.5 Hz using field stimulation. Dual-wavelength emissions of Indo-1 upon excitation at 340 nm were recorded at 405–440 and 505–540 nm using photomultiplier tubes, and, after correction for background fluorescence, free $[Ca^{2+}]_i$ was calculated as previously described (Baartscheer et al., 1996).

SR calcium content was analyzed by using rapid cooling with ice-cold (0–1°C) Tyrode's solution, which typically results in depletion of calcium from the SR, with the released calcium remaining confined to the cytoplasm (Bers, 1987). Data were collected from at least three independent differentiations per condition.

SUPPLEMENTAL INFORMATION

Supplemental Information includes Supplemental Experimental Procedures and five figures and can be found with this article online at http://dx.doi.org/10.1016/j.stemcr.2013.11.008.

ACKNOWLEDGMENTS

We thank Richard Davis, Stefan Braam, and Dorien Ward for advice and protocols for the spin EB differentiation method, and for discussions about the data. We also thank Arie Verkerk for help with manuscript preparation, and David Hood (York University, Ontario, Canada) for the *PGC-1α* promoter plasmid. This research was support by grants from the Human Frontiers Research Program (M.B.), European Research Council (ERC 323182 to C.M.), ZonMW Animal Alternatives (114000101 to S.C.), Netherlands Institute of Regenerative Medicine (M.B.), Rembrandt Institute of Cardiovascular Science (C.M. and G.K.), Netherlands Genomics Initiative (NGI/NWO 05040202 to P.M.), and Marie Curie IRG 247918 (to P.M.). The Seahorse Extracellular Flux Analyzer was purchased with the generous contribution of Dorpmans-Wigmans Stichting. C.L.M. is a cofounder and consultant of Pluriomics bv.

Received: August 15, 2013
Revised: November 14, 2013
Accepted: November 14, 2013
Published: December 12, 2013

REFERENCES

Arany, Z., He, H., Lin, J., Hoyer, K., Handschin, C., Toka, O., Ahmad, F., Matsui, T., Chin, S., Wu, P.-H., et al. (2005). Transcriptional coactivator PGC-1 alpha controls the energy state and contractile function of cardiac muscle. Cell Metab. *1*, 259–271.

Baartscheer, A., Schumacher, C.A., Opthof, T., and Fiolet, J.W.T. (1996). The origin of increased cytoplasmic calcium upon reversal of the Na+/Ca(2+)-exchanger in isolated rat ventricular myocytes. J. Mol. Cell. Cardiol. *28*, 1963–1973.

Baartscheer, A., Schumacher, C.A., Coronel, R., and Fiolet, J.W.T. (2011). The driving force of the Na^+/Ca^{2+}-exchanger during metabolic inhibition. Front Physiol *2*, 10.

Bassani, J.W., Bassani, R.A., and Bers, D.M. (1994). Relaxation in rabbit and rat cardiac cells: species-dependent differences in cellular mechanisms. J. Physiol. *476*, 279–293.

Bates, M.G.D., Bourke, J.P., Giordano, C., d'Amati, G., Turnbull, D.M., and Taylor, R.W. (2012). Cardiac involvement in mitochondrial DNA disease: clinical spectrum, diagnosis, and management. Eur. Heart J. *33*, 3023–3033.

Bers, D.M. (1987). Ryanodine and the calcium content of cardiac SR assessed by caffeine and rapid cooling contractures. Am. J. Physiol. *253*, C408–C415.

Bers, D.M. (2008). Calcium cycling and signaling in cardiac myocytes. Annu. Rev. Physiol. *70*, 23–49.

Birket, M.J., Orr, A.L., Gerencser, A.A., Madden, D.T., Vitelli, C., Swistowski, A., Brand, M.D., and Zeng, X. (2011). A reduction in ATP demand and mitochondrial activity with neural differentiation of human embryonic stem cells. J. Cell Sci. *124*, 348–358.

Campeau, E., Ruhl, V.E., Rodier, F., Smith, C.L., Rahmberg, B.L., Fuss, J.O., Campisi, J., Yaswen, P., Cooper, P.K., and Kaufman, P.D. (2009). A versatile viral system for expression and depletion of proteins in mammalian cells. PLoS ONE *4*, e6529.

Christoffels, V.M., Mommersteeg, M.T.M., Trowe, M.-O., Prall, O.W.J., de Gier-de Vries, C., Soufan, A.T., Bussen, M., Schuster-Gossler, K., Harvey, R.P., Moorman, A.F.M., and Kispert, A. (2006). Formation of the venous pole of the heart from an Nkx2-5-negative precursor population requires Tbx18. Circ. Res. *98*, 1555–1563.

Davis, R.P., van den Berg, C.W., Casini, S., Braam, S.R., and Mummery, C.L. (2011). Pluripotent stem cell models of cardiac disease and their implication for drug discovery and development. Trends Mol. Med. *17*, 475–484.

Dubois, N.C., Craft, A.M., Sharma, P., Elliott, D.A., Stanley, E.G., Elefanty, A.G., Gramolini, A., and Keller, G. (2011). SIRPA is a specific cell-surface marker for isolating cardiomyocytes derived from human pluripotent stem cells. Nat. Biotechnol. *29*, 1011–1018.

Elliott, D.A., Braam, S.R., Koutsis, K., Ng, E.S., Jenny, R., Lagerqvist, E.L., Biben, C., Hatzistavrou, T., Hirst, C.E., Yu, Q.C., et al. (2011). NKX2-5(eGFP/w) hESCs for isolation of human cardiac progenitors and cardiomyocytes. Nat. Methods *8*, 1037–1040.

Fritah, A., Steel, J.H., Nichol, D., Parker, N., Williams, S., Price, A., Strauss, L., Ryder, T.A., Mobberley, M.A., Poutanen, M., et al. (2010a). Elevated expression of the metabolic regulator receptor-interacting protein 140 results in cardiac hypertrophy and impaired cardiac function. Cardiovasc. Res. *86*, 443–451.

Fritah, A., Christian, M., and Parker, M.G. (2010b). The metabolic coregulator RIP140: an update. Am. J. Physiol. Endocrinol. Metab. *299*, E335–E340.

Goldhaber, J.I., Ji, S., Lamp, S.T., and Weiss, J.N. (1989). Effects of exogenous free radicals on electromechanical function and metabolism in isolated rabbit and guinea pig ventricle. Implications for ischemia and reperfusion injury. J. Clin. Invest. *83*, 1800–1809.

Graham, B.H., Waymire, K.G., Cottrell, B., Trounce, I.A., MacGregor, G.R., and Wallace, D.C. (1997). A mouse model for mitochondrial myopathy and cardiomyopathy resulting from a deficiency in the heart/muscle isoform of the adenine nucleotide translocator. Nat. Genet. *16*, 226–234.

Guerra, L., Cerbai, E., Gessi, S., Borea, P.A., and Mugelli, A. (1996). The effect of oxygen free radicals on calcium current and dihydropyridine binding sites in guinea-pig ventricular myocytes. Br. J. Pharmacol. *118*, 1278–1284.

Gurung, I.S., Medina-Gomez, G., Kis, A., Baker, M., Velagapudi, V., Neogi, S.G., Campbell, M., Rodriguez-Cuenca, S., Lelliott, C., McFarlane, I., et al. (2011). Deletion of the metabolic transcriptional coactivator PGC1β induces cardiac arrhythmia. Cardiovasc. Res. *92*, 29–38.

Hirano, M., Davidson, M., and DiMauro, S. (2001). Mitochondria and the heart. Curr. Opin. Cardiol. *16*, 201–210.

Irrcher, I., Ljubicic, V., and Hood, D.A. (2009). Interactions between ROS and AMP kinase activity in the regulation of PGC-1alpha transcription in skeletal muscle cells. Am. J. Physiol. Cell Physiol. *296*, C116–C123.

Koumi, S.I., Martin, R.L., and Sato, R. (1997). Alterations in ATP-sensitive potassium channel sensitivity to ATP in failing human hearts. Am. J. Physiol. *272*, H1656–H1665.

Lai, L., Leone, T.C., Zechner, C., Schaeffer, P.J., Kelly, S.M., Flanagan, D.P., Medeiros, D.M., Kovacs, A., and Kelly, D.P. (2008). Transcriptional coactivators PGC-1alpha and PGC-lbeta control overlapping programs required for perinatal maturation of the heart. Genes Dev. *22*, 1948–1961.

Lehman, J.J., Barger, P.M., Kovacs, A., Saffitz, J.E., Medeiros, D.M., and Kelly, D.P. (2000). Peroxisome proliferator-activated receptor gamma coactivator-1 promotes cardiac mitochondrial biogenesis. J. Clin. Invest. *106*, 847–856.

Lelliott, C.J., Medina-Gomez, G., Petrovic, N., Kis, A., Feldmann, H.M., Bjursell, M., Parker, N., Curtis, K., Campbell, M., Hu, P., et al. (2006). Ablation of PGC-1β results in defective mitochondrial activity, thermogenesis, hepatic function, and cardiac performance. PLoS Biol. *4*, e369.

Leone, T.C., Lehman, J.J., Finck, B.N., Schaeffer, P.J., Wende, A.R., Boudina, S., Courtois, M., Wozniak, D.F., Sambandam, N., Bernal-Mizrachi, C., et al. (2005). PGC-1α Deficiency Causes Multi-System Energy Metabolic Derangements: Muscle Dysfunction, Abnormal Weight Control and Hepatic Steatosis. PLoS Biol *3*, e101.

Liu, M., Liu, H., and Dudley, S.C., Jr. (2010). Reactive oxygen species originating from mitochondria regulate the cardiac sodium channel. Circ. Res. *107*, 967–974.

Martin-Puig, S., Wang, Z., and Chien, K.R. (2008). Lives of a heart cell: tracing the origins of cardiac progenitors. Cell Stem Cell *2*, 320–331.

Mummery, C.L., Ward, D., and Passier, R. (2007). Differentiation of human embryonic stem cells to cardiomyocytes by coculture with endoderm in serum-free medium. Curr. Protoc. Stem Cell Biol. *2*, 1F.2.1–1F.2.14.

Mummery, C.L., Zhang, J., Ng, E.S., Elliott, D.A., Elefanty, A.G., and Kamp, T.J. (2012). Differentiation of human embryonic stem cells and induced pluripotent stem cells to cardiomyocytes: a methods overview. Circ. Res. *111*, 344–358.

Murry, C.E., and Keller, G. (2008). Differentiation of embryonic stem cells to clinically relevant populations: lessons from embryonic development. Cell *132*, 661–680.

Ng, E.S., Davis, R., Stanley, E.G., and Elefanty, A.G. (2008). A protocol describing the use of a recombinant protein-based, animal product-free medium (APEL) for human embryonic stem cell differentiation as spin embryoid bodies. Nat. Protoc. *3*, 768–776.

Nichols, C.G., Ripoll, C., and Lederer, W.J. (1991). ATP-sensitive potassium channel modulation of the guinea pig ventricular action potential and contraction. Circ. Res. *68*, 280–287.

Piquereau, J., Novotova, M., Fortin, D., Garnier, A., Ventura-Clapier, R., Veksler, V., and Joubert, F. (2010). Postnatal development of mouse heart: formation of energetic microdomains. J. Physiol. *588*, 2443–2454.

Ruas, J.L., White, J.P., Rao, R.R., Kleiner, S., Brannan, K.T., Harrison, B.C., Greene, N.P., Wu, J., Estall, J.L., Irving, B.A., et al. (2012). A PGC-1α isoform induced by resistance training regulates skeletal muscle hypertrophy. Cell *151*, 1319–1331.

Russell, L.K., Mansfield, C.M., Lehman, J.J., Kovacs, A., Courtois, M., Saffitz, J.E., Medeiros, D.M., Valencik, M.L., McDonald, J.A., and Kelly, D.P. (2004). Cardiac-specific induction of the transcriptional coactivator peroxisome proliferator-activated receptor γ coactivator-1α promotes mitochondrial biogenesis and reversible cardiomyopathy in a developmental stage-dependent manner. Circ. Res. *94*, 525–533.

Scarpulla, R.C., Vega, R.B., and Kelly, D.P. (2012). Transcriptional integration of mitochondrial biogenesis. Trends Endocrinol. Metab. *23*, 459–466.

Schaper, J., Schwarz, F., Kittstein, H., Kreisel, E., Winkler, B., and Hehrlein, F.W. (1980). Ultrastructural evaluation of the effects of global ischemia and reperfusion on human myocardium. Thorac. Cardiovasc. Surg. *28*, 337–342.

St-Pierre, J., Drori, S., Uldry, M., Silvaggi, J.M., Rhee, J., Jäger, S., Handschin, C., Zheng, K., Lin, J., Yang, W., et al. (2006). Suppression of reactive oxygen species and neurodegeneration by the PGC-1 transcriptional coactivators. Cell *127*, 397–408.

Straight, A.F., Cheung, A., Limouze, J., Chen, I., Westwood, N.J., Sellers, J.R., and Mitchison, T.J. (2003). Dissecting temporal and spatial control of cytokinesis with a myosin II Inhibitor. Science *299*, 1743–1747.

Thomson, J.A., Itskovitz-Eldor, J., Shapiro, S.S., Waknitz, M.A., Swiergiel, J.J., Marshall, V.S., and Jones, J.M. (1998). Embryonic stem cell lines derived from human blastocysts. Science *282*, 1145–1147.

Ventura-Clapier, R., Garnier, A., Veksler, V., and Joubert, F. (2011). Bioenergetics of the failing heart. Biochim. Biophys. Acta *1813*, 1360–1372.

Zima, A.V., and Blatter, L.A. (2006). Redox regulation of cardiac calcium channels and transporters. Cardiovasc. Res. *71*, 310–321.